ELSEVIER

Fusion Engineering and Design 28 (1995) 596–609

Fusion Engineering and Design

Measurements of D–T neutron induced radioactivity in plasma-facing materials and their role in qualification of activation cross-section libraries and codes

A. Kumar [a], Y. Ikeda [b], M.A. Abdou [a], M.Z. Youssef [a], C. Konno [b], K. Kosako [b], Y. Oyama [b], T. Nakamura [b], H. Maekawa [b]

[a] *School of Engineering and Applied Science, University of California at Los Angeles, Los Angeles, CA 90095, USA*
[b] *Department of Reactor Engineering, Japan Atomic Energy Research Institute, Tokai, Ibraki 319-11, Japan*

Abstract

The D–T neutron-induced radioactivity constitutes one of the foremost issues in fusion reactor design. The validation of activation cross-sections and decay data libraries is one of the important requirements for validating ITER design from safety and waste disposal viewpoints. An elaborate, experimental program was initiated in 1988, under USDOE–JAERI collaborative program, to validate the radioactivity codes/libraries. The measurements of decay–γ spectra from irradiated, high purity samples of Al, Si, Ti, V, Cr, Mn–Cu alloy, Fe, Co, Ni, Cu, stainless steel 316 (AISI 316), Zn, Zr, Nb, Mo, In, Sn, Ta, W, and Pb, among others, were conducted under D–T neutron fluences varying from 1.6×10^{10} n cm^{-2} to 6.1×10^{13} n cm^{-2}. As many as 14 neutron energy spectra were covered for a number of materials. The analysis of isotopic activities of the irradiated materials using activation cross-section libraries of four leading radioactivity codes, i.e. ACT4/THIDA-2, REAC-3, DKR-ICF, and RACC, has shown large discrepancies among the calculations, on the one hand, and between the calculations and the measurements, on the other. A discussion is also presented on definition and obtention of safety cum quality factors for various activation libraries.

1. Introduction

With the Engineering Design Activity (EDA) phase of International Thermonuclear Experimental Reactor (ITER) being already on, the validation of neutron transport cross-sections and activation cross-section libraries has assumed urgency. The ITER designers are likely to need safety factors in the near term for ensuring a somewhat conservative design. Extensive measured data on induced radioactivity have been generated over past few years in the framework of a USDOE–JAERI collaborative program [1–6]. This activity on induced radioactivity measurements has been spread over the last five years and has covered, among others, a large number of plasma facing materials of interest to D–T fusion ractors, including ITER and DEMO. The experiments have consisted of irradiation of high purity material samples in a range of neutron energy spectra in simulated fusion environments of prototypical blanket assemblies driven by D–T neutrons at FNS–JAERI. A typical sample measured 10 mm in diameter by 1 mm thickness, and the neutron

Elsevier Science S.A.
SSDI 0920-3796(94)00376-9

fluence ranged from about 10^{10} n cm^{-2} to about 10^{14} n cm^{-2}, over an irradiation period of 30 min and 10 h. The irradiated samples were then cooled for varying times, from about 10 min to about 3 weeks, and their activity was derived by counting associated γ rays with intrinsic germanium detectors.

The measured isotopic γ activities were then compared with the calculations with activation cross-section libraries of widely used radioactivity codes such as DKR-ICF [7], REAC-3 [8], ACT4/THIDA-2 [9], and RACC [10]. Same decay data were used to calculate isotopic activities using these libraries. Largest discrepancies between the calculations and the experiments are seen for vanadium, copper, cobalt, nickel, molybdenum, and tungsten. For example, calculation-to-experiment (CE) ratios for ^{60}Co production from copper, nickel, and cobalt, have the following ranges: 0.1–1.3, 0.5–3.1, and 0.08–6.8 respectively. The discrepancies in calculations of the measured isotopic activities originate largely from differences in activation cross-sections of these libraries, even though, at times, uncertainty on computed neutron energy spectrum could also make a substantial contribution to these discrepancies.

The measurements of the induced radioactivity are not only useful for providing experimental data of direct use to reactor-licensing authorities, but also helpful in establishing quality of an activation cross-section library in predicting the production of radioactive isotopes of crucial importance. The large body of the measured and computed isotopic radioactivities has permitted formulation of broad conclusions as to the confidence level one can place in using one or another activation cross-section library for predicting induced radioactivity in various components of a fusion reactor design. Important activation cross-section data that are shown to be erroneous, as a result of the comparison between calculations and the experiments, could be the subject of high priority reappraisal–re-evaluation.

2. Experiments

Very extensive experiments to measure induced radioactivity were planned and executed under USDOE–JAERI collaborative program in fusion neutronics [1–6]. The experimental geometry and other details are available in the referenced publications. Generally, small disc samples (10 mm diameter by 1 mm thickness) were irradiated in typical neutron energy spectra for induced radioactivity measurements. High purity foils of magnesium, aluminum, silicon, titanium, vanadium, chromium, iron, manganese, cobalt, nickel, stainless steel 316, copper, zinc, zirconium, niobium, molybdenum, siliver, indium, tin, tantalum, tungsten, gold, and lead as well as two high temperature superconductors, namely $YBa_2Cu_3O_7$ and $ErBa_2Cu_3O_7$, were irradiated during various phases of this collaborative program. The D–T neutron fluence ranged from about 10^{10} to about 1.7×10^{15} n cm^{-2}. In all, 14 spectral locations, named alphabetically from A through N, were utilized for foil irradiations in phases IIC through IIIC of this collaborative program [6]. High resolution intrinsic germanium detectors were used for γ spectroscopy after letting the irradiated samples cool for times varying from minutes to weeks.

3. Comparison of calculation with experimental measurements

Count spectra for various irradiation times, cooling times, and neutron energy spectra for each irradiated material were processed to obtain isotopic activities. Then, neutron energy spectrum calculations were carried out using both Monte Carlo (MCNP [11]), and deterministic (DORT [12], DOT3.5 [12]) transport codes and cross-section libraries (based on ENDF/B-V [13] and JENDL [14]). The calculated spectra were then used together with the activation cross-section data libraries included with four radioactivity codes of DKR-ICF, RACC, ACT4/THIDA-2, and REAC-3 to obtain calculated isotopic activities. As compared with the work reported earlier [1–6], there are very important differences in the work being reported here. First of all, we have used only the activation cross-section libraries of the four radioactivity codes with a new radioactivity calculation module developed by us, i.e. RADCAL. This module is specifically designed to calculate isotopic activities for a given irradiated material using all usual parameters such as neutron flux, irradiation time, source neutron intensity, product half-life, decay γ yield, cooling time, activation cross-section library, material composition etc. This module was benchmarked against analytical solutions. We have used the same values of decay half-lives, isotopic composition, and decay γ yields for all the calculations. The isotopic compositions were adapted from Ref. [15], and isotopic half lives and decay γ yields were taken from Ref. [16]. Secondly, in the present work, we have covered useful experimental data for all the 14 spectral locations, called A through N. Hence, the results being reported apply to a larger span of neutron energy spectra. The comparison, CE ratio, was then obtained from the calculated and experimentally measured isotopic activities. Experi-

Table 1
Observed CE ranges for isotopic activities in irradiated samples of iron, cobalt, nickel, copper and molybdenum

Irradiated material	Radioactive isotope (product)	Observed CE ranges for various activation cross-section libraries				
		ACT4	REAC-3	DKR-ICF	RACC	All four libraries
Iron	^{56}Mn	0.88–1.10	0.77–1.07	0.90–1.13	1.01–1.22	0.77–1.22
	^{51}Cr	0.87–0.99	0.75–0.86	0.94–1.07	1.51–1.70	0.75–1.70
	^{54}Mn	1.04–1.23	0.85–0.99	0.97–1.11	1.19–1.34	0.85–1.34
Cobalt	^{56}Mn	0.90–1.42	0.91–1.20	0.93–1.26	0.93–1.27	0.90–1.42
	^{59}Fe	1.04–2.09	1.75–2.08	0.83–1.05	0.97–1.16	0.83–2.08
	^{58}Co	1.05–1.26	1.32–1.57	1.54–1.84	1.75–2.08	1.05–2.08
	^{60}Co	3.10–5.03	4.10–6.81	2.60–4.36	0.085–0.14	0.085–6.81
Nickel	^{62m}Co	1.30–1.64	1.34–1.68	1.34–1.70	missing	1.30–1.70
	^{57}Ni	0.86–1.10	0.87–1.19	1.15–1.66	1.05–1.43	0.86–1.66
	^{59}Fe	0.88–1.52	1.96–3.21	0.62–1.05	5.5×10^{-4}–9.0×10^{-4}	5.5×10^{-4}–3.21
	^{58}Co	1.09–2.00	1.19–2.26	0.55–1.28	0.94–1.55	0.55–2.26
	^{57}Co	0.88–1.22	1.20–1.53	0.91–1.32	0.25–0.33	0.25–1.53
	^{60}Co	0.81–1.39	0.78–1.31	0.53–0.88	1.89–3.10	0.53–3.10
Copper	^{62m}Co	0.6–16.5	0.6–19.1	missing	missing	0.6–19.1
	^{65}Ni	1.08–1.31	0.98–1.20	1.02–1.24	missing	0.98–1.31
	^{64}Cu	0.76–0.85	0.74–0.83	0.75–0.84	0.75–0.84	0.74–0.85
	^{60}Co	0.31–1.24	0.71–1.33	0.11–0.41	0.30–1.13	0.11–1.33
Molybdenum	^{101}Tc	1.7–2.4	1.4–2.2	1.4–2.0	1.3–2.1	1.3–2.4
	^{101}Mo	2.0–3.3	1.7–2.9	1.6–2.7	1.5–2.8	1.5–3.3
	^{91}Mo	0.7–1.9	1.7–4.2	0.9–1.8	1.7–4.2	0.7–4.2
	^{98m}Nb	1.2–1.6	1.2–1.6	missing	missing	1.2–1.6
	^{97}Nb	0.68–0.72	3.9–4.2	1.0–1.2	0.7–0.8	0.68–4.2
	^{93m}Mo	1.4–2.2	5.9–9.3	2.0–3.1	missing	1.4–9.3
	^{96}Nb	1.5–2.0	2.7–3.4	4.3–5.6	1.3–1.8	1.3–5.6
	^{99}Mo	0.99–1.12	0.81–0.93	0.89–1.02	1.11–1.27	0.81–1.27
	^{89}Zr	0.94–1.00	2.05–2.22	1.53–1.67	1.75–1.91	0.94–2.22
	^{95m}Nb	0.83–0.92	6.6–7.4	1.7–2.0	1.6–2.0	0.83–7.4
	^{92m}Nb	0.99–1.12	1.06–1.17	1.0–1.2	1.1–1.4	0.99–1.4
	^{95}Nb	1.02–1.10	2.37–2.55	2.4–2.7	0.7–0.9	0.7–2.7
	^{91}Nb	1.4–1.7	3.04–3.45	1.3–1.6	3.1–3.7	1.3–3.7
	^{95}Zr	0.4–0.6	1.03–1.25	1.0–1.3	0.6–0.8	0.4–1.3

mental error was factored in while obtaining the CE ratios.

3.1. Calculation-to-experiment ratio trends

The ratios of the computed and experimental isotopic activities, available from all the four libraries, have been obtained for a number of neutron energy spectra for all the irradiated materials. However, we will be presenting the range of CE ratios for each isotopic product for only few of those materials to explain the trends. For a given material, overall CE ratio dispersion trends are being presented. Note that overall dispersion for an isotopic product is obtained by obtaining the lowest and the highest CE ratios observed for its activity by the four libraries for all the spectral locations covered in the analysis. One standard deviation of experimental error is considered in determining the overall dispersion. Table 1 shows observed CE ratio discrepancies for some of the materials.

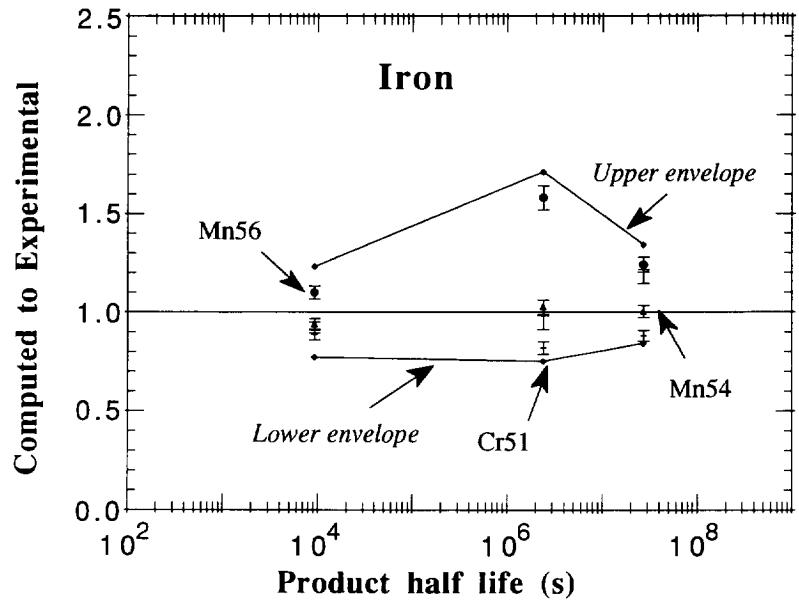

Fig. 1. Iron: CE ratio dispersion for isotopic activities using activation cross-sections in libraries of ACT4, DKR-ICF, RACC, and REAC-3.

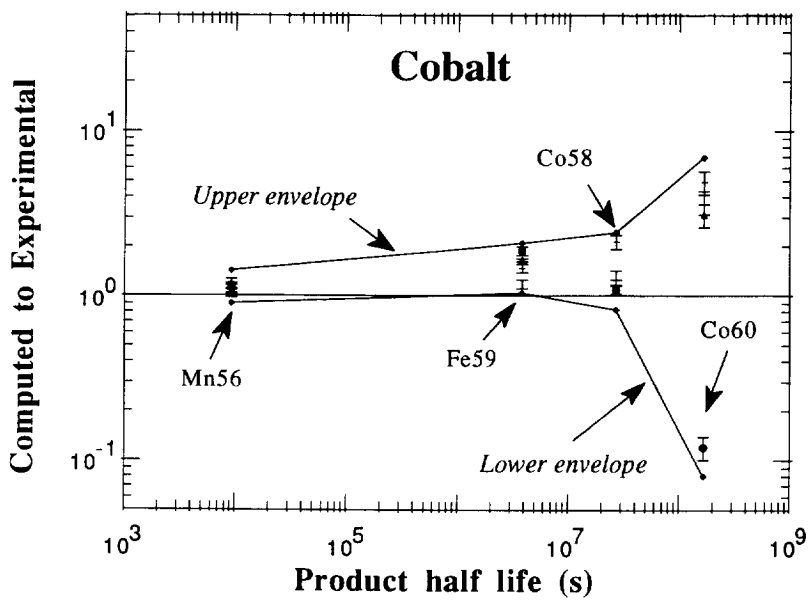

Fig. 2. Cobalt: CE ratio dispersion for isotopic activities using activation cross-sections in libraries of ACT4, DKR-ICF, RACC, and REAC-3.

3.1.1. Iron

Fig. 1 is a plot of CE ratios for iron. The data for three spectral locations, i.e. A, F, and L, are considered. Results with ENDF/B-VI, JENDL-3, and JEF-2 cross-sections are also included for ^{54}Mn. Upper envelope represents a curve that joins the largest CE ratios for each

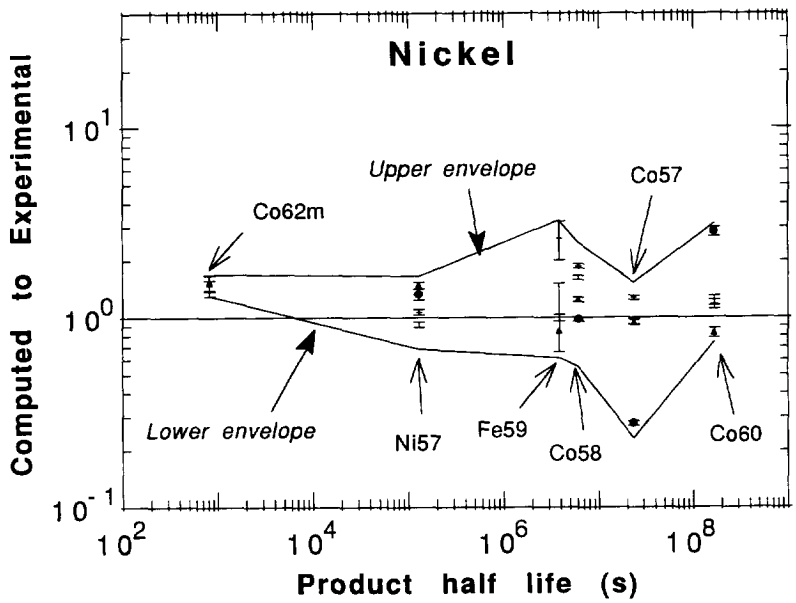

Fig. 3. Nickel: CE ratio dispersion for isotopic activities using activation cross-sections in libraries of ACT4, DKR-ICF, RACC, and REAC-3.

isotope; lower envelope, on the contrary, passes through the lowest CE ratios. The cross-section for $^{54}Fe(n,\alpha)^{51}Cr$ reaction is significantly off in REAC-3, DKR-ICF, and RACC libraries, being underpredicted at higher energy in REAC-3, and overpredicted in RACC above about 10 MeV. The shape of this cross-section differs sharply from that of those in ENDF/B-VI, JENDL-3, and JEF-2. The cross-section shape for $^{54}Fe(n,p)^{54}Mn$ in RACC differs sharply from those in ENDF/B-VI, JENDL-3, and JEF-2 libraries.

3.1.2. Cobalt

Fig. 2 is a plot of CE ratios for cobalt. The data for two spectral locations, i.e. A and C, are considered. Results with ENDF/B-VI, JENDL-3, and JEF-2 (same as ENDF/B-VI) cross-sections are also included for ^{59}Fe. JENDL-3 and ENDF/B-VI cross-sections differ significantly from each other for $^{59}Co(n,2n)^{58}Co$; REAC-3 comes closest to JENDL-3 and ENDF/B-VI; ACT4 and DKR-ICF cross-sections differ a lot from all others. As for $^{59}Co(n,\gamma)^{60}Co$, all the four libraries have different cross-sections. However, ACT4 and RACC have peculiar representations for this reaction; the cross-section in RACC is constant at less than 10^{-2} barn below about 1 MeV. The ACT4 cross-section above 3 MeV drops rapidly and is lower by a factor of 4 or more than the smallest cross-section at about 14 MeV. It is to be noted that RACC library does not have cross-section data for $^{59}Co(n,2n)^{58m}Co$ and $^{59}Co(n,\gamma)^{60m}Co$ reactions, which contribute to production of ^{58}Co and ^{60}Co respectively. REAC-3 has clear trends for large overprediction for ^{59}Fe, ^{58}Co, and ^{60}Co.

3.1.3. Nickel

Fig. 3 is a plot of CE ratios for nickel. The data for three spectral locations, i.e. A, B, and K, are considered. Results with ENDF/B-VI, JENDL-3, and JEF-2 (same as ENDF/B-VI) cross-sections are also included for ^{57}Ni. JENDL-3 and ENDF/B-VI cross-sections do not differ significantly from each other for $^{58}Ni(n,2n)^{57}Ni$ below 16 MeV. All the libraries have rather coarse group structure in the energy range of interest for this reaction to allow making any unambiguous judgment as to the quality of the cross-sections. However, the cross-sections in DKR-ICF and RACC are considerably above those from ENDF/B-VI, JENDL-3 and other libraries. This can explain the tendency of both these libraries to overpredict CE ratios for $^{58}Ni(n,2n)^{57}Ni$. As for $^{58}Ni(n,p)^{58}Co$, all the four libraries have different cross-sections and deviate from ENDF/B-VI. The cross-sections for $^{60}Ni(n,p)^{60}Co$ differ a lot from each other; the cross-section in DKR-ICF appears to be much lower than that in other libraries between 10 and 15 MeV.

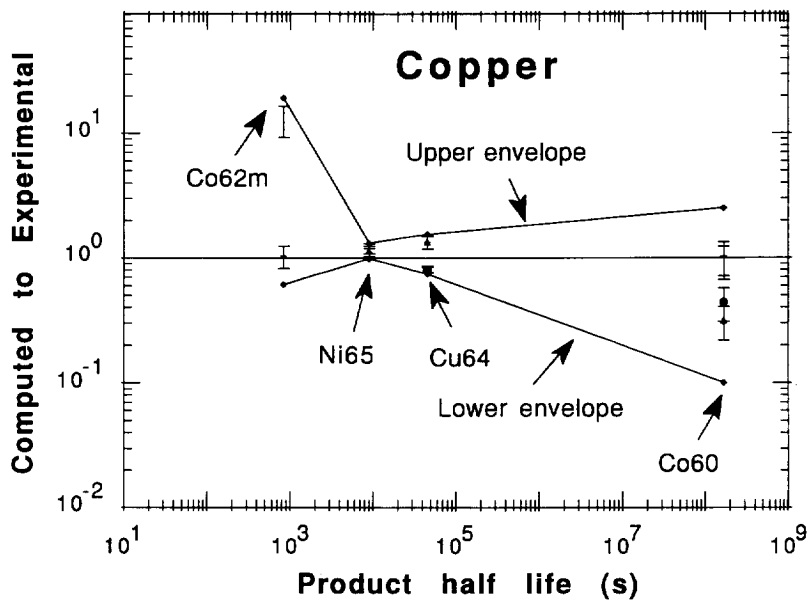

Fig. 4. Copper: CE ratio dispersion for isotopic activities using activation cross-sections in libraries of ACT4, DKR-ICF, RACC, and REAC-3.

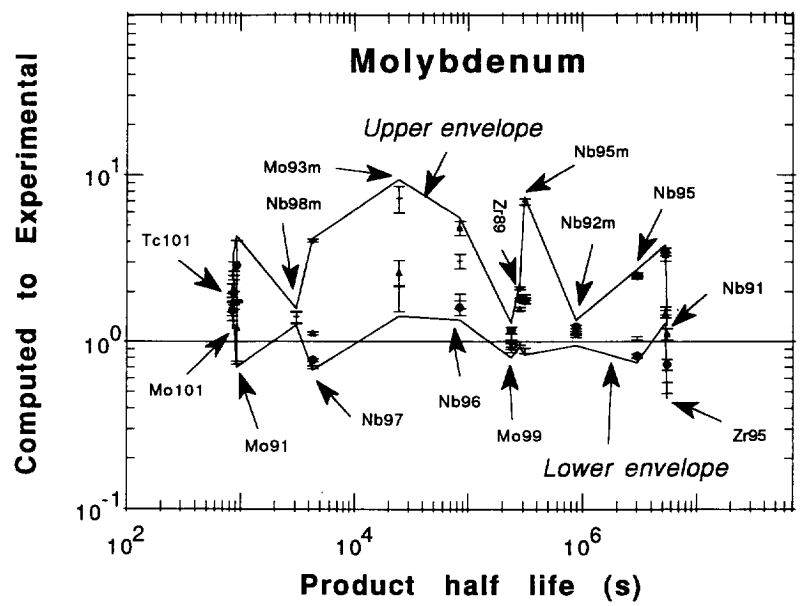

Fig. 5. Molybdenum: CE ratio dispersion for isotopic activities using activation cross-sections in libraries of ACT4, DKR-ICF, RACC, and REAC-3.

RACC library does not have cross-sections for $^{62}Ni(n,p)^{62m}Co$ and $^{58}Ni(n,p)^{58m}Co$ reactions. The cross-section for $^{62}Ni(n,\alpha)^{59}Fe$ reaction is too low. The production rate of ^{59}Fe is 3 orders of magnitude lower than those of other libraries. REAC-3 systematically overpredicts ^{59}Fe production. There are two contribu-

tors behind this trend: (i) largest cross-section for $^{62}Ni(n,\alpha)^{59}Fe$ reaction, (ii) large value for $^{60}Ni(n, 2p)^{59}Fe$ reaction from REAC-3, as much as about 30% of total ^{59}Fe production. In fact, this reaction channel is absent in other three libraries. As for ^{58}Co, the sum of the cross-sections for $^{58}Ni(n,p)^{58m}Co$ and $^{58}Ni(n, p)^{58}Co$ reactions is the lowest for RACC, a factor of about 2 or more as compared with that from the other three libraries. The contribution of $^{58}Ni(n,np+d)^{57}Co$ to ^{57}Co production is approximately a factor of 4 lower compared with other libraries. The contribution of $^{60}Ni(n,p)^{60m}Co$ to ^{60}Co production is approximately a factor of 4 higher compared with other libraries.

3.1.4. Copper

Fig. 4 is a plot of CE ratios for copper. The data for two spectral locations, i.e. A and K, are considered. All the four libraries have different cross-sections and deviate from ENDF/B-VI for a number of important reactions. In fact, both ACT4 and DKR-ICF have cross-sections for $^{63}Cu(n,\alpha)^{60}Co$ reaction that are much lower than those in ENDF/B-VI, REAC-3, and RACC. As for ^{60}Co, the sum of the cross-sections for $^{63}Cu(n,\alpha)^{60m}Co$ and $^{63}Cu(n,\alpha)^{60}Co$ reactions is quite low for DKR-ICF. This explains the trend of systematically low CE values for this library for ^{60}Co. Regarding CE ratio dispersion of ^{62m}Co, it appears that the experimental data for the spectral location A, that lead to CE ratios lying towards the upper envelope, might be in error. The cross-section data for ACT4 and REAC-3 libraries for $^{65}Cu(n,\alpha)^{62m}Co$ yield calculation results that lie within 15% of each other. Both DKR-ICF and RACC libraries do not have cross-section data for $^{65}Cu(n,\alpha)^{62m}Co$ and well as $^{63}Cu(n,\alpha)^{60m}Co$, the latter reaction being an important contributor to the production of ^{60}Co. In addition, RACC library does not have cross-sections for $^{65}Cu(n,p)^{65}Ni$.

3.1.5. Molybdenum

Fig. 5 is a plot of CE ratios for molybdenum. The data for two spectral locations, i.e. A and C, are considered. RACC library does not have cross-sections for $^{92}Mo(n,2n)^{91m}Mo$ and $^{94}Mo(n,2n)^{93m}Mo$. It is to be noted that ^{91}Nb is produced by β^- decay of ^{91}Mo. Wide divergences are observed in the cross-sections in all the libraries. We see important differences among CE ratios from different libraries. On ^{93m}Mo production predictability, there are two contributing channels: $^{94}Mo(n,2n)^{93m}Mo$ and $^{92}Mo(n,\gamma)^{93m}Mo$. Only two libraries, i.e. ACT4 and REAC-3, have cross-sections for $^{92}Mo(n,\gamma)^{93m}Mo$ channel. The fractional contributions from this channel in the two libraries are very different. For example, for spectrum A, the fractional contributions of $^{92}Mo(n,\gamma)^{93m}Mo$ channel are about 0.2% and

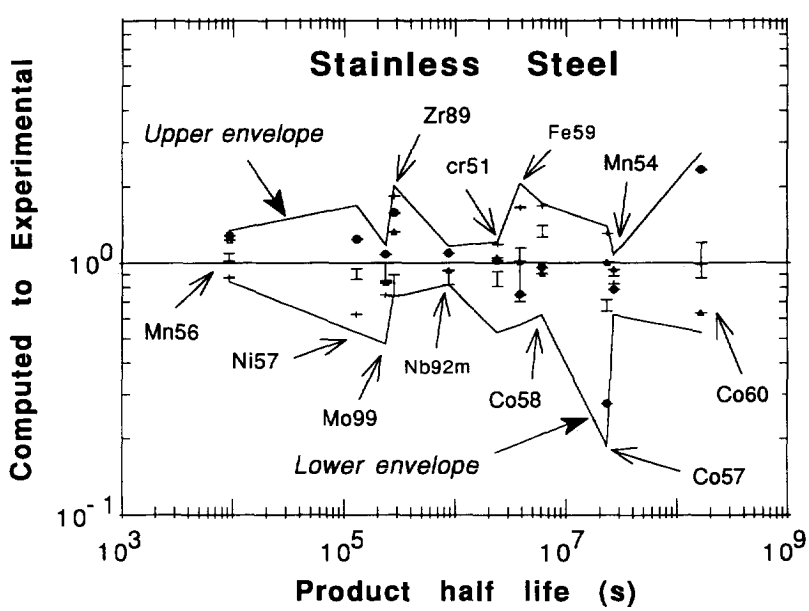

Fig. 6. Stainless steel 316: CE ratio dispersion for isotopic activities using activation cross-sections in libraries of ACT4, DKR-ICF, RACC, and REAC-3.

about 75% for ACT4 and REAC-3 respectively. The cross-sections for $^{92}Mo(n,\gamma)^{93m}Mo$ reactions in the two libraries do not only differ by orders of magnitude, but also have divergent energy-wise dependence. In fact, ACT4 shape does not conform to usual trends of an (n,γ) reaction at lower neutron energies. Usually, the cross-section for such reactions has $1/v$ dependence at low neutron energies.

As for ^{89}Zr, both DKR-ICF and RACC do not have cross-section for $^{92}Mo(n,\alpha)^{89m}Zr$ channel. However, in spite of this, these two libraries together with REAC-3 have a systematic tendency to overpredict CE ratios, because of significantly larger $^{92}Mo(n,\alpha)^{89}Zr$ channel in all these three libraries. In fact, the library-wise contributions to ^{89}Zr from $^{92}Mo(n,\alpha)^{89}Zr$ alone, in descending order, are (i) RACC, (ii) DKR-ICF, (iii) REAC-3, and (iv) ACT4. In fact, overall, ACT4 yields the best CE ratios. For ^{91}Mo, both DKR-ICF and RACC libraries do not have cross-sections for $^{92}Mo(n,2n)^{91m}Mo$ channel. In spite of this, RACC yields the largest CE ratios for ^{91}Mo. REAC-3 shows almost as much as about 36% of contribution from $^{92}Mo(n,2n)^{91m}Mo$ channel; for ACT4, this channel contributes about 3% only. In fact, the cross-section for this channel from REAC-3 is an order of magnitude larger than that from ACT4. For ^{96}Nb, DKR-ICF library yields a factor of 3–4 higher results than other three libraries for $^{96}Mo(n,p)^{96}Nb$ channel. REAC-3 appears to have excessive contributions from three secondary channels, i.e. $^{97}Mo(n,np)^{96}Nb$, $^{97}Mo(n,d)^{96}Nb$, and $^{98}Mo(n,t)^{96}Nb$. In fact, the primary channel $^{96}Mo(n,p)^{96}Nb$ contributes only as much as about 50% by REAC-3, as against about 94% by ACT4. All the libraries overpredict ^{96}Nb production.

For ^{95m}Nb, REAC-3 has the largest cross-section for $^{95}Mo(n,p)^{95m}Nb$ channel, whereas ACT4 has the lowest cross-section. In fact, REAC-3, DKR-ICF, and RACC predict much larger contributions from this channel compared with that by ACT4, the overprediction being as much as a factor of 2–5 larger. REAC-3 has large contributions from secondary channels too. These channels contribute as much as about 50% in REAC-3, whereas in ACT4 it amounts to about 10% only. For ^{95}Nb, the trends observed for ^{95m}Nb have important impact, as $^{95m}Nb \rightarrow {}^{95}Nb$ channel makes a significant contribution. DKR-ICF predicts too large contribution by $^{95}Mo(n,p)^{95}Nb$ channel. In fact, the contribution by this library is about 2.5 times that by ACT4. REAC-3, again, has large contributions from the secondary channels; their contribution is as much as about 30% to the total. For ^{97}Nb, one discovers very peculiar trends with all the libraries when one looks very closely at the finer, channel-wise decomposition. Even though CE ratio ranges predicted by ACT4 and RACC are rather close, the channel-wise contributions are widely different even for these two libraries. For example, for $^{97}Mo(n,p)^{97}Nb$ channel, RACC has the lowest contribution. The RACC contribution is almost about 70% of ACT4 contribution. However, for secondary channels of $^{98}Mo(n,np$ or $d)^{97}Nb$, RACC contribution is as much as about 2.5 times that by ACT4. For ACT4, the secondary channels contribute about 20%; they contribute respectively about 45%, about 30%, and about 55% for RACC, DKR-ICF, and REAC-3.

3.1.6. Stainless steel 316

Fig. 6 is a plot of CE ratios for stainless steel. The data for three spectral locations, i.e. A, B, and C, are considered. The CE ratio dispersions are especially large for ^{57}Ni, ^{89}Zr, ^{99}Mo, ^{59}Fe, ^{58}Co, ^{57}Co, and ^{60}Co. Primarily, the trends observed for the steel components, i.e. Fe, Ni, Mn, Mo, and Co, are reflected in these figures. However, there could be compensating or complicating effects arising as a result of competing reaction channels from these component materials. As for ^{51}Cr, the competing reaction channels come from Cr and Fe, e.g. $^{52}Cr(n,2n)^{51}Cr$ and $^{50}Cr(n,\gamma)^{51}Cr$ from Cr, and $^{54}Fe(n,\alpha)^{51}Cr$ from Fe. ^{56}Mn receives contributions from Fe, Mn, and Co. ^{58}Co has contributions from Co and Ni. ^{59}Fe receives contributions from three materials, e.g. Co, Ni, and Fe. ^{54}Mn receives comparable contributions from Fe and Mn. ^{60}Co receives contributions from Ni, and Co.

4. Contributing factors to discrepancies between calculations and experiments

Both the calculation and measurement carry varying degrees of uncertainty.

4.1. Experimental errors

As for errors on measurements, it needs to be emphasized that a number of parameters affect counting statistics. The important parameters include neutron flux, half-life of γ emitter, detector efficiency, cooling time, counting time, activation cross-section, atom density, and sum-peak correction. We also need to use tabulated half-lives and decay–γ yields to convert measured counts' spectra to isotopic activities. Any errors on these quantities add to overall errors. Processing of count spectra with a large number of peaks could, at times, be detrimental to weaker peaks at lower γ energies owing to large Compton background. Thus, one

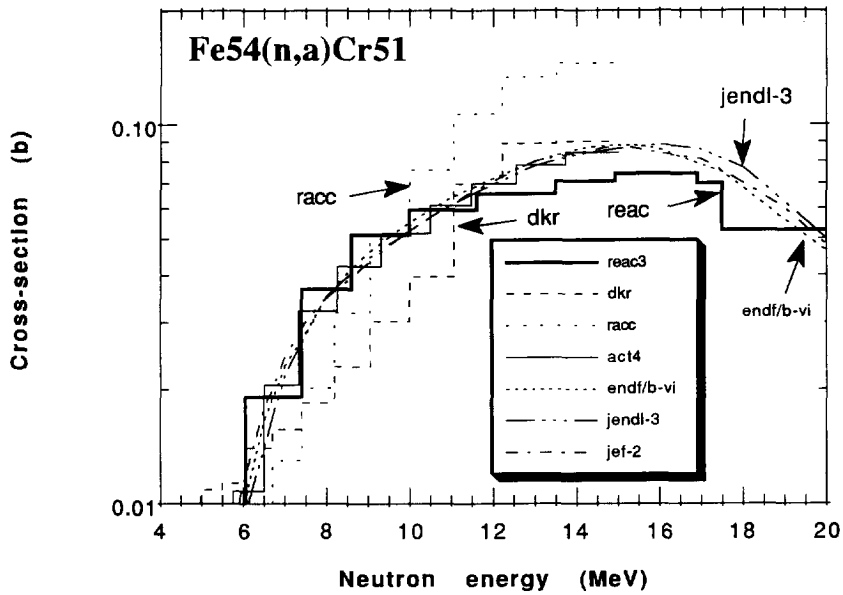

Fig. 7. Cross-sections for $^{54}Fe(n,\alpha)^{51}Cr$ from different libraries.

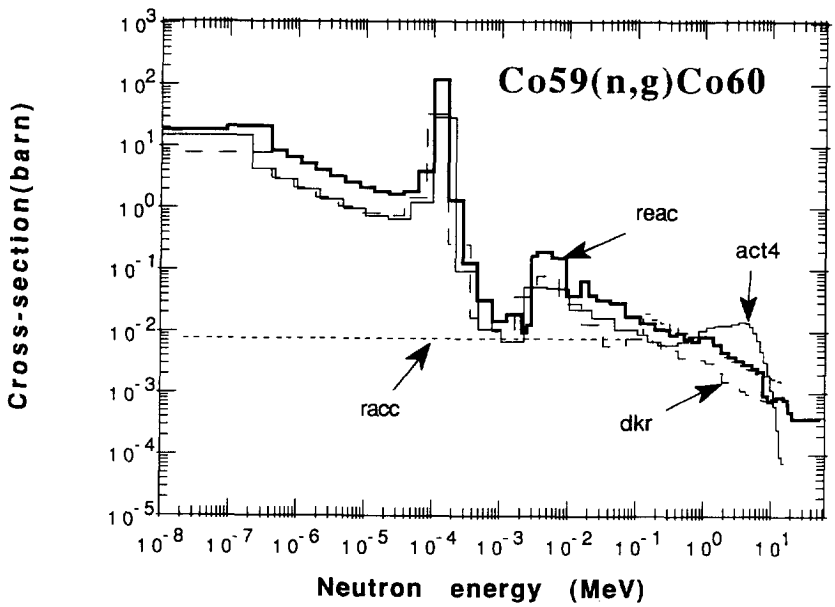

Fig. 8. Cross-sections for $^{59}Co(n,\gamma)^{60}Co$ from different libraries.

could expect to see relatively significant errors on the weak peaks. Clearly, it is not possible to furnish a single figure for even one sample material. For great majority of the measurements, the error lies between about 2% and about 15%.

4.2. Calculational errors

Let us understand the roles of an activation cross-section, say $\sigma(E)$, and neutron energy spectrum, say $\Phi(E)$, in contributing to saturation activity, say S,

Table 2
Cross-sectional integrals for iron, cobalt, nickel, copper and molybdenum

Material	Reaction	Cross-sectional integral, CSI (barn)				Reference CSI (barn)
		ACT4	REAC-3	DKR-ICF	RACC	
Iron	$^{54}Fe(n,p)^{54}Mn$	0.700	0.683	0.736	0.411	0.661 [a] 0.700 [b] 0.760 [c]
	$^{54}Fe(n,\alpha)^{51}Cr$	4.54×10^{-2}	4.50×10^{-2}	5.64×10^{-2}	5.91×10^{-2}	4.68×10^{-2} [a] 4.53×10^{-2} [b] 4.64×10^{-2} [c]
	$^{56}Fe(n,p)^{56}Mn$	6.26×10^{-2}	6.74×10^{-2}	6.94×10^{-2}	6.89×10^{-2}	
Cobalt	$^{59}Co(n,\gamma)^{60m}Co$	174.9	196.6	72.2	no data	
	$^{59}Co(n,\gamma)^{60}Co$	109.3	267.6	54.4	0.150	
	$^{59}Co(n,\gamma)^{58m}Co$	7.06×10^{-2}	9.17×10^{-2}	0.111	no data	
	$^{59}Co(n,2n)^{58}Co$	8.26×10^{-2}	0.144	4.74×10^{-2}	0.130	0.135 [a] 0.137 [b]
	$^{59}Co(n,\alpha)^{56}Mn$	1.19×10^{-2}	1.33×10^{-2}	1.19×10^{-2}	1.33×10^{-2}	
	$^{59}Co(n,p)^{59}Fe$	3.55×10^{-2}	3.75×10^{-2}	3.75×10^{-2}	6.36×10^{-2}	3.48×10^{-2} [a] 3.51×10^{-2} [b]
Nickel	$^{58}Ni(n,2n)^{57}Ni$	3.09×10^{-3}	3.09×10^{-3}	5.74×10^{-3}	4.07×10^{-3}	3.08×10^{-3} [a] 2.97×10^{-3} [b]
	$^{64}Ni(n,\gamma)^{65}Ni$	9.12	15.9	2.97	5.05	
	$^{58}Ni(n,p)^{58m}Co$	0.201	0.417	0.441	no data	
	$^{58}Ni(n,p)^{58}Co$	0.791	0.790	0.441	0.450	
	$^{58}Ni(n,np+d)^{57}Co$	0.127	0.162	0.157	3.75×10^{-2}	
	$^{60}Ni(n,p)^{60m}Co$	0.105	6.04×10^{-2}	6.50×10^{-2}	2.74×10^{-2}	
	$^{60}Ni(n,p)^{60}Co$	6.72×10^{-2}	0.103	6.50×10^{-2}	9.17×10^{-2}	
	$^{62}Ni(n,\alpha)^{59}Fe$	1.81×10^{-3}	1.03×10^{-3}	7.72×10^{-3}	1.27×10^{-6}	
Copper	$^{63}Cu(n,\alpha)^{60m}Co$	1.30×10^{-2}	3.13×10^{-2}	no data	no data	2.58×10^{-2} [a]
	$^{63}Cu(n,\alpha)^{60}Cu$	1.00×10^{-2}	3.13×10^{-2}	1.03×10^{-2}	2.55×10^{-2}	
	$^{65}Cu(n,2n)^{64}Cu$	0.199	0.196	0.225	0.203	0.198 [a]
	$^{63}Cu(n,\gamma)^{64}Cu$	30.2	52.7	10.9	12.7	
Molybdenum	$^{92}Mo(n,2n)^{91}Mo$	2.06×10^{-2}	1.79×10^{-2}	2.11×10^{-2}	4.55×10^{-2}	
	$^{92}Mo(n,2n)^{91m}Mo$	1.02×10^{-3}	1.79×10^{-2}	no data	no data	
	$^{95}Mo(n,p)^{95m}Nb$	3.01×10^{-3}	1.75×10^{-2}	7.01×10^{-3}	6.94×10^{-3}	
	$^{96}Mo(n,p)^{96}Nb$	5.88×10^{-3}	7.48×10^{-3}	2.83×10^{-2}	5.28×10^{-3}	
	$^{94}Mo(n,2n)^{93m}Mo$	8.37×10^{-4}	5.51×10^{-4}	9.57×10^{-4}	no data	

[a] From ENDF/B-VI cross-sections; [b] From JENDL-3 cross-sections; [c] From JEF-2 cross-sections.

expressed as follows:

$$S = \int_0^\infty \Phi(E)\sigma(E)\,dE \approx \sum_{i=1}^{n} \Phi_i \sigma_i \Delta u_i$$

$$\approx \sum_{i=1}^{n} \Phi_i (\mathrm{CSI})_i \qquad (1)$$

Here $(\mathrm{CSI})_i$ is used to define another useful quantity CSI as follows:

$$\mathrm{CSI} = \sum_{i=1}^{n} (\mathrm{CSI})_i = \sum_{i=1}^{n} \sigma_i \Delta u_i \qquad (2)$$

Subscript represents ith energy group out of a total of n. Φ_i is neutron energy spectrum in energy group i and is defined per unit lethargy. Δu_i is magnitude of lethargy change for group i. CSI stands for "cross-sectional integral". Ideally, there should be a very large number of energy groups so as to describe accurately the fine features of both the activation cross-section and the spectrum. In reality, one is forced to restrict the number of energy groups. If the number of energy groups is low or the energy group boundaries are inappropriately chosen, one would have a significant contribution to the

uncertainty on S from this source alone. The maximum uncertainty in S can be expressed as

$$\left|\frac{\Delta S}{S}\right|_{\max} = \sum_{i}^{n} |P_i| \left(\left|\frac{\Delta \sigma_i}{\sigma_i}\right| + \left|\frac{\Delta \Phi_i}{\Phi_i}\right| \right) \quad (3)$$

where P_i is to be understood as integrated sensitivity for energy group i, and is given as

$$P_i = \frac{\sigma_i \Phi_i}{\sum_{k=1}^{n} \sigma_k \Phi_k \, \Delta u_k} \Delta u_i = \mathrm{PD}_i \, \Delta u_i \quad (4)$$

It follows from Eq. (3) that one needs to have relative uncertainties $|\Delta\sigma_i/\sigma_i|$ and $|\Delta\Phi_i/\Phi_i|$ on activation cross-section as well as spectrum in addition to differential sensitivity profile, say PD_i, to determine relative uncertainty on the saturation activity S.

As for impact of uncertainty in neutron energy spectrum on calculation of a saturation activity, we estimated it by comparing the calculations using ENDF/B-V-based (US) and JENDL-3-based (Japanese) spectra. Usually, the saturation activities lay within about 10% of one another. As hinted a number of times in Section 3.1, we saw large differences in both the shapes and the values of the cross-sections in various libraries for a large number of reactions. Figs. 7 and 8 provide examples of differences for $^{54}\mathrm{Fe(n,\alpha)}^{51}\mathrm{Cr}$, a threshold reaction, and $^{59}\mathrm{Co(n,\gamma)}^{60}\mathrm{Co}$, a capture reaction, respectively. Fig. 7 also shows cross-sections from ENDF/B-VI and JENDL-3 compilations. It is clear that one can expect large deviations in cross-sections for threshold as well as capture reactions. Not only that, we also found that there were no activation cross-sections for a number of reactions in some of the libraries. In spite of observing such large differences, one might speculate whether these point-wise differences in cross-sections would not somehow cancel out when looking at an energy-integrated quantity such as S. In this respect, it is useful to look at CSI defined by Eq. (2). Physical significance of CSI for a particular isotopic activity can be inferred from the fact that, for a flat spectrum (in lethargy space), the integral response S is directly determined by CSI. Table 2 compares CSI values obtained from ACT4, REAC-3, DKR-ICF, and RACC libraries for important reactions in iron, cobalt, nickel, copper, and molybdenum. In fact, one could state that there is a very large difference in the CSI values, from different libraries, for an average reaction. Thus, one could easily expect large dispersion in CE ratio values from activation cross-sections alone, as was amply brought out in Section 3.1.

5. Probability density of calculation-to-experimental ratio

It is evident from the preceding sections that there is substantial disagreement between calculation and the experimental measurements for almost all the materials. The inadequacies in neutron transport cross-sections, methodology of transport solver, and geometrical–material modeling of irradiated assembly are notable contributors to uncertainties in calculated spectra. The designers of a fusion machine need reliable information on induced radioactivity in its various components.

5.1. Safety–quality factor

The designers accept the inadequacies of modeling and cross-section data and incorporate safety factors to come up with a somewhat conservative design [17–18]. Ideally, one needs to correct the calculation using a multiplier, such that the corrected prediction is equal to actual (experimental) amounts of induced activity. This correction factor for a code (and library) can be defined as

$$\text{Ideal corrective multiplier (ICM)} = 1/(\text{CE ratio}) \quad (5)$$

where inverse of observed CE ratios defines correction factor (ICM) for a given material. As long as one has access to very large amount of CE ratio data for each material, one can obtain the ICM and associated confidence level. In practice, it is almost impossible to obtain the ICM as defined above because of problems associated with (i) impossibility of exact modeling of the experimental assembly, (ii) non-vanishing errors of the calculational method–code, and (iii) finite experimental error. Thus, one will rather be dealing with a distribution of correction factors. If this distribution is statistically reliable, one can set a confidence level and obtain a correction factor which, when multiplied by the calculated value, yields a corrected calculational result that will be equal to or greater than the experimental value for ensuring overprediction, or the reverse if underprediction of integral response will be required. We prefer to call such a multiplier a safety factor. For all practical purposes, safety factor can be seen as a quality factor too.

Let us now develop a formulation that will be useful for later discussion. Imagine that we have a number M of CE ratio results on integral response S. Also, there is an associated error δ(CE ratio) with each CE ratio result. For convenience, variable CE ratio is represented by a variable z. z is allowed to vary from 0 to infinity. We divide this z variable space into L discrete

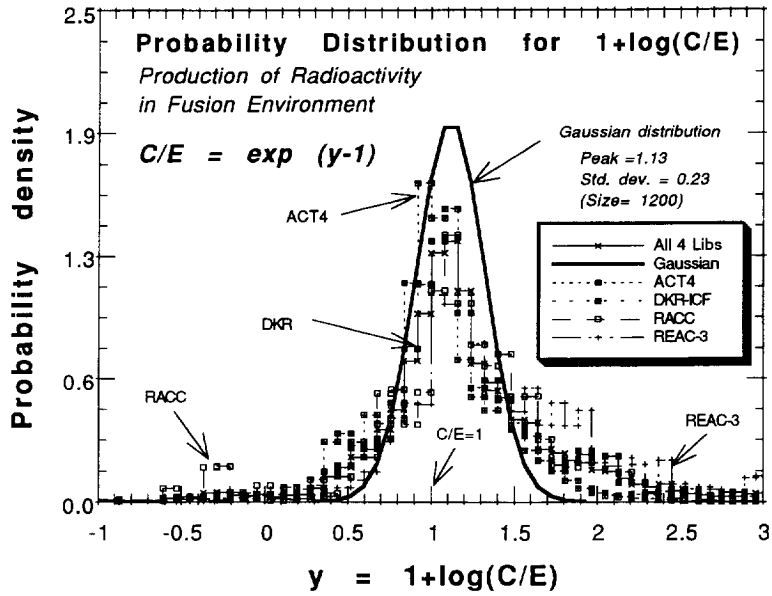

Fig. 9. Probability density of CE ratios expressed as a function of $y = 1 + \log(\text{CE ratio})$ for ACT4, DKR-ICF, RACC and REAC-3 libraries.

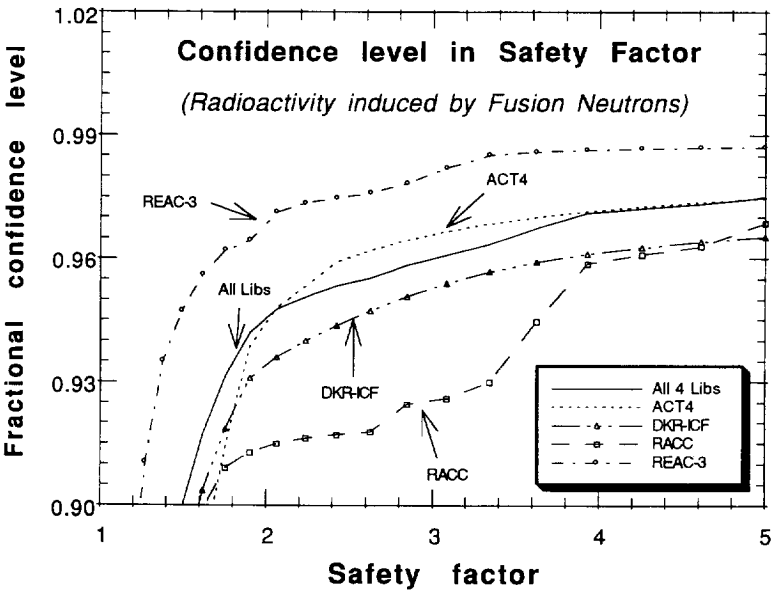

Fig. 10. Fractional confidence level as a function of safety factor for ACT4, DKR-ICF, RACC, and REAC-3 libraries (for ensuring that there is no underprediction of radioactivity induced by D–T neutrons).

bins bounded by z_k ($k = 0-L$). We then bin the observed CE ratio results, say z_{resi} ($i = 1-M$), over the L discrete bins. $\delta(z_{resi})$, the error assigned to ith CE ratio result z_{resi}, and its distribution function are to be taken into account while binning the z_{resi} data. For example, when error is distributed normally, one uses a gaussian

distribution function, centered at z_{resi} and characterized by a full width determined by $\delta(z_{resi})$, to distribute z_{resi}. Once all M results for CE ratio have been distributed over L bins, we normalize the distribution such that when it is integrated over entire z space one obtains unity for the resultant integral. Let us call this distribution function $\Psi(z)$. This function will satisfy the following equality:

$$\int_0^\infty \Psi(z)\,\mathrm{d}z = 1 \equiv \int_0^\infty \Psi(\text{CE ratio})\,\mathrm{d}(\text{CE ratio}) \qquad (6)$$

Let us further define what we call confidence level Ω associated with a particular value of CE ratio, say p, such that there are two situations as below:

$$\Omega(\text{CE ratio} \leqslant p) = \int_0^p \Psi(z)\,\mathrm{d}z \equiv \int_0^p \Psi(\text{CE ratio})\,\mathrm{d}(\text{CE ratio}) \qquad (7)$$

and

$$\Omega(\text{CE ratio} \geqslant p) = \int_p^\infty \Psi(z)\,\mathrm{d}z \equiv \int_p^\infty \Psi(\text{CE ratio})\,\mathrm{d}(\text{CE ratio}) \qquad (8)$$

Confidence level from Eq. (7) characterizes all CE ratios that do not exceed p, and that from Eq. (8) similarly characterizes all CE ratios that equal or exceed p. If $\Psi(z)$ were to follow normal distribution, a relative standard deviation on Ω would be given as

$$\delta(\Omega) = \frac{1}{(M\Omega)^{1/2}} \qquad (9)$$

Then, one can assign a safety factor such that

$$\text{safety factor} = \frac{1}{p} \quad (\text{with } \Omega \text{ by Eq. (7) or Eq. (8)}) \qquad (10)$$

From the foregoing, it is obvious that the ICM (Eq. (5)) and safety factor (Eq. (10)) would be identical if $\Psi(z)$ were a Dirac delta function centered at $z = \text{CE ratio} = p$. It follows that if one were to ensure overprediction of a calculated integral response, one would determine the associated confidence level from Eq. (8). For underprediction of the calculated response, one would instead use Eq. (7). However, the safety factor in either situation would be given by Eq. (10).

5.2. Distribution function

A designer could be interested in ascertaining quality of an activation cross-section library. In principle, a separate quality factor can be associated with each library if all other parameters are held constant. One can obtain a probability density distribution of CE ratios, irrespective of type of isotopic activity, sample material, or neutron energy spectrum. Theoretically, CE ratio would vary from 0 to ∞. It is useful to define another variable y, such that

$$y = 1 + \log(\text{CE ratio}) \qquad (11)$$

and

$$\text{CE ratio} = \exp(y - 1) \qquad (12)$$

y will vary from $-\infty$ to $+\infty$, for CE ratio varying from 0 to $+\infty$. There are two advantages in doing this transformation: (i) one practically contracts the independent variable space, and (ii) one can directly compare such a probability density distribution with a gaussian distribution. Five such probability distributions have been obtained: one each for each of the four libraries (ACT4, REAC-3, DKR-ICF, RACC), and a consolidated distribution for all the four libraries combined together. These probability distribution functions are shown as a function of y in Fig. 9. Also shown in the same figure is a gaussian distribution. This gaussian distribution is obtained such that (i) CE ratio of its peak is same as that of the peak in the actual distribution, and (ii) its full width at half-maximum is the same as that of the peak in the actual distribution. It follows from the figure that away from the peak the actual distribution differs widely from the gaussian. There are huge disagreements among the four libraries in entire range of CE ratios. Fig. 10 shows confidence level as a function of safety factor. It is evident that the confidence level improves very slowly beyond safety factor value of 2.

6. Nuclear data improvement vs. safety factor

Although a designer could apply safety factors or quality factors as discussed in the preceding section, the problems afflicting a calculational model or activation cross-sections would not go away. In fact, in long term, it would be required to solve these problems unless one were willing to pay excessive economic costs that are directly linked to the conservatism inherent in the use of safety factors. As for additional integral measurements for induced radioactivity for ITER, the need is very obvious because improvement of the activation cross-sections over entire energy range is practically impossible in the next five to ten years owing to acute paucity of required resources. These measurements,

however, need to be strongly complemented by the cross-section evaluators who would have to prioritize their work in response to immediate ITER requirements. For example, those activation cross-sections that lead to largest CE ratio discrepancies on isotopic activities and are important for ITER receive top priority.

7. Summary and conclusions

Recently concluded USDOE–JAERI collaboration on induced radioactivity experiments has brought out large disagreements between calculations and measurements for a large number of materials of relevance to ITER. The contributing factors responsible for this disagreement are topped by discrepant activation cross-section data. The CE results for various isotopic activities were processed to obtain probability distribution functions, confidence levels and safety factors for various activation libraries. Finally, it was pointed out that, even though the designers might need to use appropriate safety factors, it is strongly advised to strengthen the activity in the area of the integral measurements of the induced radioactivity. In parallel, the cross-section evaluators should be requested to reorganize their activities so as to respond to top priority needs first.

Acknowledgment

The US contribution was supported by the US Department of Energy, Office of Fusion Energy, under Contract DE-FG03-86ER52123.

References

[1] A. Kumar, M.A. Abdou, Y. Ikeda and C. Konno, Radioactivity and nuclear heating measurements for fusion applications, Fusion Technol. (1990) 872–876.

[2] Y. Ikeda, C. Konno, T. Nakamura, A. Kumar and M.A. Abdou, Experiment on induced activities and decay-heat in simulated D–T neutron fields: JAERI-USDOE collabortive program on fusion neutronics, Fusion Technol. 19 (1991) 1961.

[3] A. Kumar, M.A. Abdou, Y. Ikeda and T. Nakamura, Analysis of induced activities measurements related to decay-heat in phase IIC experimental assembly: USDOE/JAERI collaborative program on fusion neutronics experiments, Fusion Technol. 19 (1991) 1909.

[4] A. Kumar, M.Z. Youssef, Y. Ikeda and C. Konno, Experiments and analysis for measurements of decay-heat related induced activities in simulated line source driven d–t neutron fields of phase IIIA: USDOE/JAERI collaborative program on fusion neutronics experiments, Fusion Technol. 19 (1991) 1859.

[5] Y. Ikeda, C. Konno, Y. Oyama, T. Nakamura, A. Kumar, M.Z. Youssef and M.A. Abdou, Experimental verification of the current data and methods for induced radioactivity and decay heat calculation in D–T fusion reactors, Fusion. Eng. Des. 18 (1991) 387.

[6] A. Kumar, Y. Ikeda, M.A. Abdou, M.Z. Youssef, C. Konno, K. Kosako, Y. Oyama, T. Nakamura and H. Maekawa, Induced radioactivity measurements in fusion neutron environment: joint report of USDOE/JAERI collaborative program on fusion neutronics, Reps. UCLA-ENG-91-32/UCLA-FNT-53 and JAERI-M-93-018, February 1993.

[7] D.L. Henderson and O. Yasar, A radioactivity and dose rate calculation code package, Vols. 1 and 2, RSIC computer code collection, CCC-323, April 1987.

[8] F.M. Mann, REAC*2: Users Manual and Code Description, WHC-EP-0282, Westinghouse Hanford Company, 1989.

[9] Y. Seki et al., THIDA-2: an advanced code system for calculation of transmutation, activation, decay heat and dose rate, RSIC computer code collection, CCC-410, April 1987.

[10] J. Jung, Theory and use of the radioactivity code RACC, ANL/FPP/TM-122, Argonne National Laboratory, 1979.

[11] J.F. Briesmeister (ed.), MCNP—A general Monte Carlo code for neutron and photon transport: version 3A, Rep. LA-7396-M, Rev. 2, September 1988; MCNP3B Newsl. Los Alamos National Laboratory, July 18, 1988.

[12] W.A. Rhoades and R.L. Childs, DOT-IV version 4.3: one and two dimensional transport code collection, RSIC computer code collection CCC-429, May 1984.

[13] R.E. MacFarlane, TRANSX-CTR: a guide for interfacing MATXS cross-section libraries to nuclear transport codes for fusion systems analysis, Los Alamos National Laboratory, Rep. LA-9863-MS, February 1984.

[14] Y. Seki and H. Iida, Coupled 42-group neutron and 21-group gamma-ray cross section sets for fusion reactor calculations, JAERI-M 8818, 1980.

[15] C.M. Lederer and V.S. Shirley, Table of Isotopes, Wiley, New York, 7th edn., 1978.

[16] E. Browne and R.B. Firestone, in V.S. Shirley (ed.), Table of Radioactive Isotopes, Wiley–Interscience, New York, 1986.

[17] M.E. Sawan and L.A. El-Guebaly, Three-dimensional neutronics analysis for the U.S. magnet shield of ITER, Fusion Technol. 19 (1991) 1469.

[18] L.A. El-Guebaly, Overview of the US-ITER magnet shield: concept and problems, Fusion Technol. 19 (1991) 1475.